Effect of Electrode Adhesion Strength on Lithium-ion Battery Performance

Undergraduate Honors Thesis

Presented in Partial Fulfillment of the Requirements for Graduation with Distinction in the Department of Mechanical Engineering at The Ohio State University

By

John Kim

Undergraduate Program in Aeronautical and Astronautical Engineering

The Ohio State University

2020

Thesis Committee

Jung Hyun Kim, Ph.D., Advisor

Hanna Cho, Ph.D.

Abstract

Lithium-ion batteries (LIBs) have applications ranging from small electronic devices to big battery packs used in electric vehicles. Although commercial batteries have good performance, they have low volumetric density and low active material utilization and high cost of production. To address this, increasing the thickness of the electrode (>200 μm) beyond the conventional thickness (~60 μm) is a promising approach. Thick electrodes have more active materials packed in a given volume thereby improving energy density and reducing the amount of inactive materials to lower the cost of production. Good adhesion properties at the interface of electrode and substrate are crucial for achieving the desired battery performance. Improper adhesion is caused due to various reasons including generation of internal stress, mismatch of surface energies, etc. Particularly in thick electrodes, which are desirable for high energy density, adhesion strength is a critical factor for performance. Although a few groups have explored the adhesion properties of LIB electrodes, their effect on the performance and the parameters affecting the adhesion have not been studied. The conventional 180° mechanical peel test is a well-known technique to measure adhesion strength by peeling away the electrode from the current collector. In this research, the impact of various parameters such as the thickness of the electrode, binder material, viscosity of the slurry, and different current collectors on the adhesion strength of the electrode are studied through systematic experiments and the corresponding variation in battery performance is reported.

Acknowledgments

First, I want to give my special thanks to my advisor, Dr. Jung-Hyun Kim, who provided me with an opportunity to participate in the undergraduate research program. Transitioning from Aerospace Engineering coursework to a completely new battery field was new and challenging for me, and Dr. Kim and his graduate students supported me very well. Dr. Kim gave me guidance throughout the research, gave pathways to my thesis topic, and provided assistance whenever needed.

I also want to thank Lalith Rao, a graduate research assistant in Dr. Kim's lab. He provided me assistance with lab-work and assisted in teaching me detailed knowledge for thick electrodes. Lalith also provided data for a part of my research to assist in achieving the final results.

Table of Contents

Abstract iii
Acknowledgments iv
List of Tables vii
List of Figures viii
Chapter 1. Introduction 10
1.1 Introduction of Lithium-ion Battery 10
1.2 Introduction of Thick Electrode 13
1.3 Focus of Research 17
1.4 Significance of Research 18
1.5 Overview of Thesis 19
Chapter 2. Experiments 20
2.1: Preliminary Experiment 20
2.2: Methodology 22
2.3: Parameters 28
2.3.1: Substrate 30
2.3.2: Thickness 33
2.3.2: Parameters- Binder 35
2.4: Mechanical Peel Test 37
Chapter 3. Results and Discussions 39
3.1: SEM Test for Composite Binder 39
3.2: Peel Test Results 40
3.3 Electrochemical Results 42

3.3.1 Substrate Testing 42
3.3.2 Thickness Testing 44
3.3.3 Binder Testing 46
Chapter 4. Conclusion 49
4.1 Summary 49
4.2 Contribution 50
4.3 Future Work 51
Bibliography 52

List of Tables

Table 1. Sample Table 30
Table 2. Consistent Parameters for Substrate Testing 33
Table 3. Consistent Parameters for Thickness Testing 35
Table 4. Consistent Parameters for Binder Testing 37

List of Figures

Figure 1. Lithium-ion Battery Schematic (Source: Research Gate) 11
Figure 2. Battery Production Process (Source: Research Gate) 12
Figure 3. Energy Density of Li-ion (Park, 2012) 13
Figure 4. Thick Electrode Schematic (Source: 24M) 14
Figure 5. Thick Electrode Transport Distance (Source: Research Gate) 15
Figure 6. Novel Thick Electrode (Source: Kuang, 2019) 16
Figure 7. Crack Formed Thick Electrode Schematic 16
Figure 8. Mechanical Delamination in Thick Electrodes (Source: Lee, 2018) 17
Figure 9. Preliminary Experiment: Cycle Test 21
Figure 10. Preliminary Experiment: Rate Capability Test 21
Figure 11. Thinky ARV-310 Planetary Centrifugal Vacuum Mixer 22
Figure 12. Slurry Coating Process 24
Figure 13. Doctor Blade (MTI Corp.) 24
Figure 14. Heat Rolling Press with Variable Speed (MTI Corp.) 24
Figure 15. Argon-filled Glove Box (LC Technology) 26
Figure 16. Coin Cell Production Schematic 26
Figure 17. Arbin Battery Cycler (Arbin Instruments) 27
Figure 18. Design of Experiment 28
Figure 19. Effect of Each Parameter on Adhesion 29
Figure 20. Sample I: Al Substrate 31
Figure 21. Sample II: C-Al 32
Figure 22. Example Sample: E-Al 33
Figure 23. Sample III: 100 µm 34
Figure 24. Sample IV: 250 µm 34
Figure 25. Sample V: 400 µm 35
Figure 26. Binder Chemistry Samples 36
Figure 27. Peel Test Schematic 38
Figure 28. Tensile Strength machine and Test Set-Up 38
Figure 29. SEM image of LFP with Composite Binder scaled at (a) 10 µm (b) 5 µm (c) 10 mm 39
Figure 30. Sample Output from Peel Test 40
Figure 31. Peel Test Results 41
Figure 32. Substrate: Discharge Capacity vs. C-Rate Graph 43
Figure 33. Substrate: Voltage vs. Specific Capacity Graph 44
Figure 34. Thickness: Discharge Capacity vs. C-Rate Graph 45
Figure 35. Thickness: Voltage vs. Specific Capacity Graph 46
Figure 36. Binder: Discharge Capacity vs. C-Rate Graph 47

Figure 37. Binder: Voltage vs. Specific Capacity Graph..... 48

Chapter 1. Introduction

1.1 Introduction of Lithium-ion Battery

Lithium-ion battery (LIBs) is a commonly used rechargeable energy storage system that requires chemical reactions, oxidation, and reduction to store energy. LIB consists of three main components: cathode, anode, and electrolyte/separator. The cathode material consists of active material, binder, and conductive carbon, each having a crucial role for battery performance. The active material provides the lithium metal oxide, which can store and send the lithium ions to create a charge. The binder is used for bonding and to hold the material together. The conductive carbon is used for electrochemical conductivity by providing an electron conduction pathway from the substrate to the electrode. The anode is a storage for lithium ions and where the electrons are created via lithium-ion transportation. In a discharging state, a lithium-ion stored inside the anode (negative side) is transferred with the electrolyte through the separator to the cathode (positive side). This process creates a free electron in the anode, which is then delivered to the device being charged. The separator blocks the internal transportation of the electron and advocates the electron to be separated. This cycle repeats and works vice-versa in the charging state, which completes the rechargeable battery. [1]

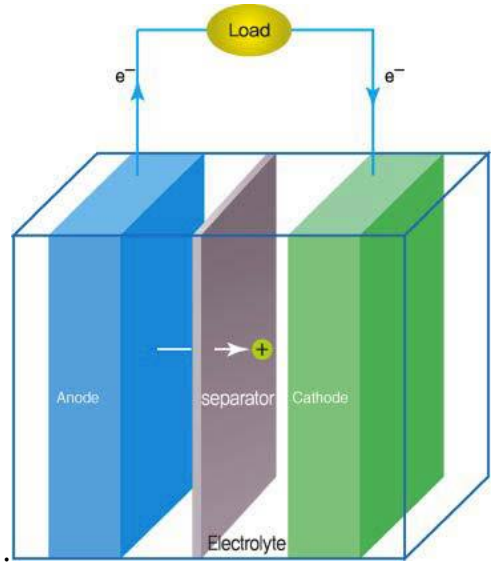

Figure 1. Lithium-ion Battery Schematic (Source: Research Gate)

The construction of a lithium-ion battery consists of many steps. First, the slurry material is prepared by mixing the active material, binder and conductive agent in specific mass ratios to create the cathode. This slurry is coated onto a current collector and is left to dry. Once dried, the material goes through a process called calendaring. In this process, the electrodes are compressed by pushing through a heat-rolled system. The electrodes are punched into circular shapes for the construction of coin cells. The cell is then assembled by stacking electrodes on each other, held apart by the separator. The electrolyte is injected to ensure the lithium-ion transportation. Figure 2 below summarizes the whole production process.

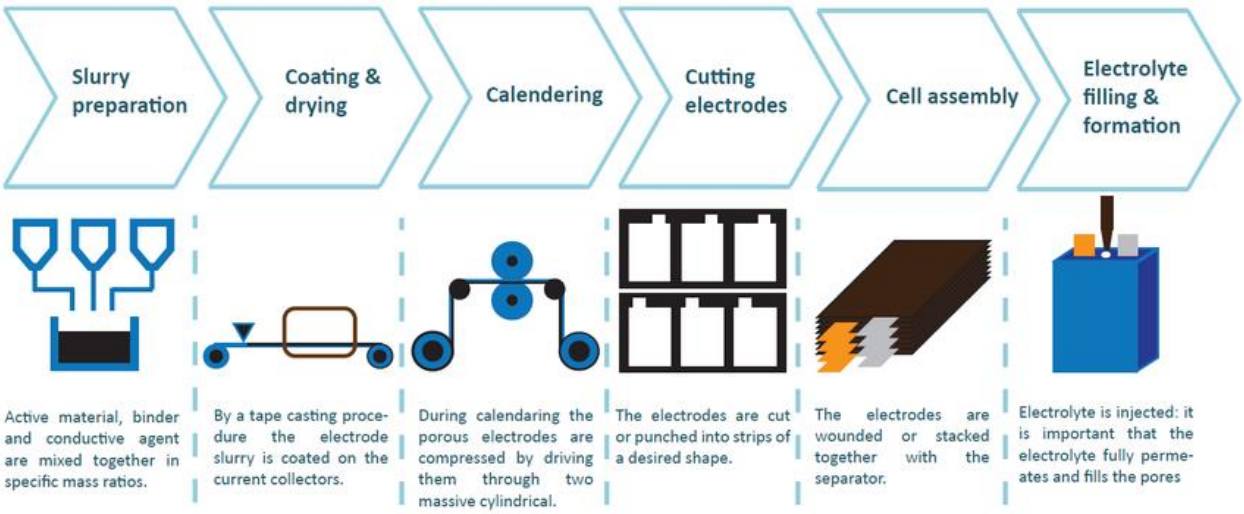

Figure 2. Battery Production Process (Source: Research Gate)

Lithium-ion batteries have been commercialized for a few decades and the discovery of lithium-ion was substantial to the battery field. Before the discovery of lithium-ions, batteries were made of much worse-performing material like nickel-cadmium and lead-acid. The lithium-ion showed to have better energy density and specific energy than any other materials previously used and a new generation battery that was much thinner and higher in voltage was developed. The lithium ion's specification allowed for the commercialization of batteries used in small portable devices such as cell phones and laptops.

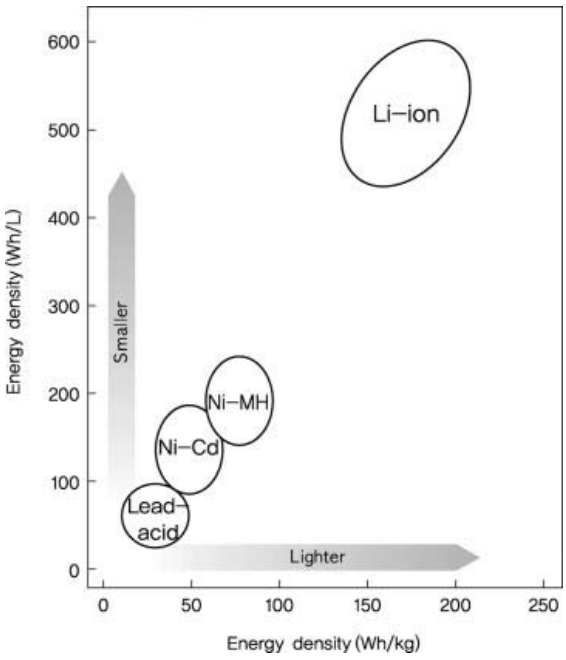

Figure 3. Energy Density of Li-ion (Park, 2012)

Before, the primary focus of LIB research was completed on small electric appliances. For many years now, the focus of LIB research has been towards large applications like electric vehicle uses and energy storage systems. LIBs currently used in commercial electric vehicle far lacks the performance and the cost of production compared to traditional internal combustion engine-powered cars. To overcome these limitations, utilizing thick active material will ensure the improvement in the energy density of the cell and the reduction of production cost. The simple concept of storing more active materials, thus increasing the volume ratio, reducing the electrode porosity, and decreasing the content of inactive materials, is proved to be one effective approach to lowering the cost of production and improving battery performance.

1.2 Introduction of Thick Electrode

The current limitations of LIBs are low volumetric density, low active material utilization, and high cost of production. To overcome these problems, the perfect solution

applied in this study is the application of thick electrodes. Thick electrode application implies the simple concept of storing more active materials into a single cell to improve the energy density. Thick electrode also utilizes less inactive materials as compared to thin electrodes which advocates in lower cost of production. As seen in Figure 4., the thick electrode utilizes much more active material in a single cell, and much less inactive materials such as separators and current collectors, which ultimately results in higher battery performance and lower production cost. [2]

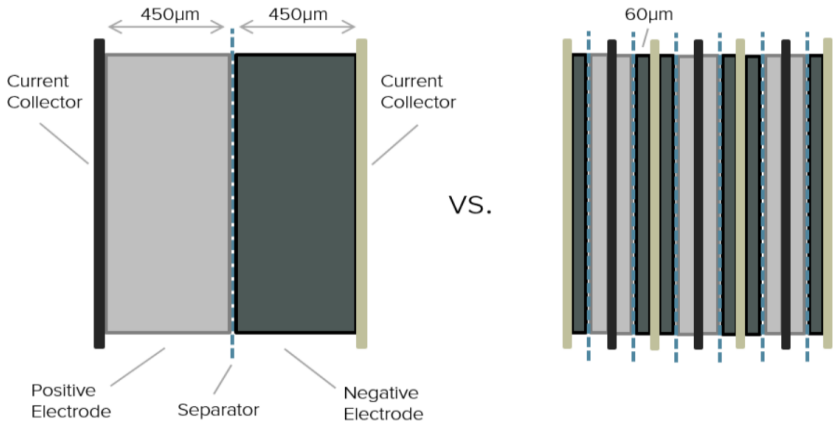

Figure 4. Thick Electrode Schematic (Source: 24M)

Studies have shown that simply using a thicker electrode results in worse performance than thin electrodes. When the battery is in an active state and the electrolyte is carrying the ions from one end to another, the thick electrode requires more lithium-ion transport distance. As seen in Figure 5 below, the thick electrode requires a longer lithium-ion transport distance than a thin electrode.

Figure 5. Thick Electrode Transport Distance (Source: Research Gate)

This long Li-ion transport distance obstructs the travel and restricts the ions from reaching the bulk of the electrodes and limits the electrolyte availability which accelerates the degradation reactions. [3]

To overcome this issue, a solution utilized in this research is the creation of vertical channels. By creating physical channels in between the thick active material, the li-ion transportation is improved thus allowing the electrolyte to penetrate to the bulk of the electrode. Multiple studies are describing how these channels could be created, including using laser-cutting, 3-D printing, magnetic templating by aligning the microstructure, etc. Figure 6 shows a visual limitation of conventional thick electrodes, and how the creation of vertical channels can address these problems.

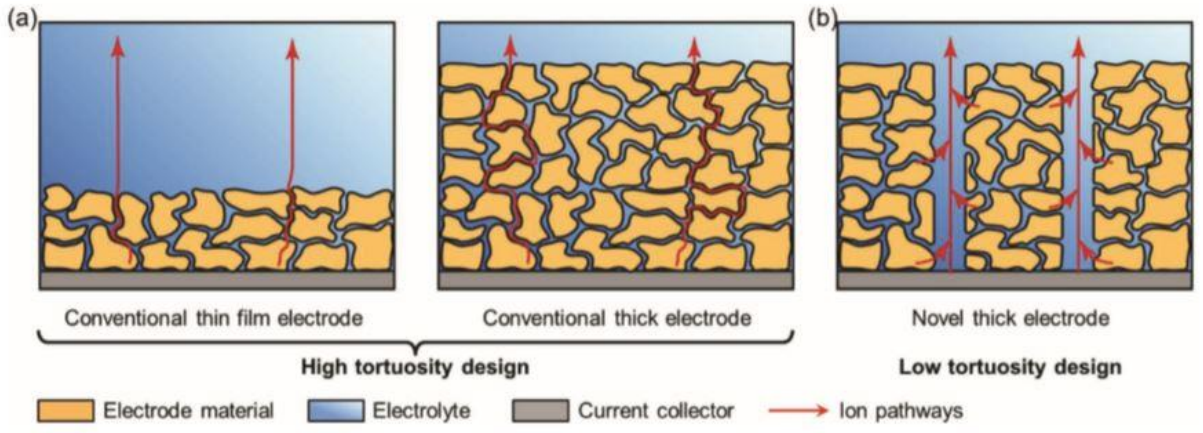

Figure 6. Novel Thick Electrode (Source: Kuang, 2019)

The process used to create these channels in this study is the crack formation in thick electrodes. Crack formation occurs to a can be formed in-situ for the thick electrode application by controlling battery production parameters including drying speed, slurry composition, and binder chemistry. These cracks can be generated from the surface of thick electrodes to the current collector thus providing vertical channels for the Li ions to travel through. [4] As shown in Figure 7, multiple cracks are generated in between the electrode materials which creates space for the Li-ion carrying electrolyte to flow through and deliver to the bulk of the electrode. This has been proved to be one effective approach to solving the limitations of thick electrodes.

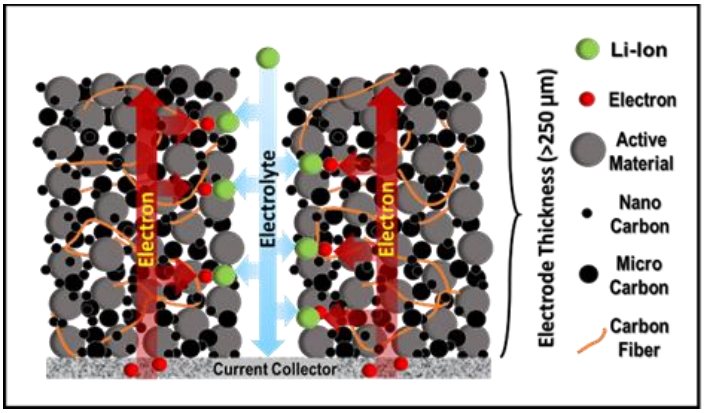

Figure 7. Crack Formed Thick Electrode Schematic

Crack formation develops another problem of internal mechanical delamination. This delamination, or separation, may appear between the active material and current collector if the adhesion strength is unsatisfactory. [5] This weak adhesion strength can be shown during the fabrication process if a mismatch of surface energy between the electrode and the current collector appears, a constant expansion of electrode material happens, etc. Figure 8 shows mechanical delamination due to bad adhesion strength of the electrode. The damage from delamination is irreversible and can result in a capacity loss. Good adhesion properties within the electrode composite and its interface with the current collector should be well maintained to deliver the designed energy and power throughout the service period [6]. Therefore, a study of electrode adhesion strength is substantial and analyzed in this paper.

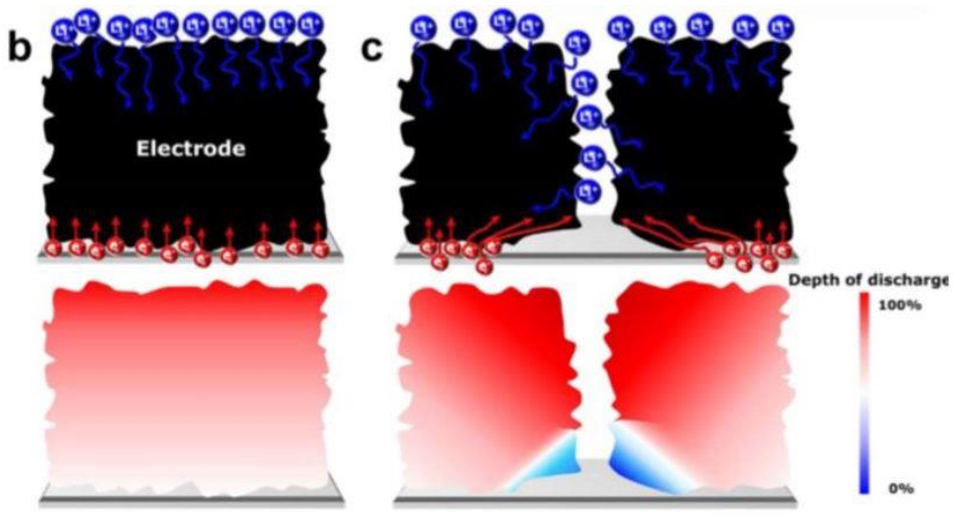

Figure 8. Mechanical Delamination in Thick Electrodes (Source: Lee, 2018)

1.3 Focus of Research

In this research, I investigated the effect of electrode adhesion strength on lithium-ion battery performance in thick electrodes. As described above, the study of adhesion strength is

substantial in thick electrode applications. I designed multiple electrodes varying multiple parameters and tested for the adhesion force and electrochemical performance for each. The adhesion force was measured by performing a mechanical peel test and the electrochemical test was measured with the rate capability test. The testing procedure is described in Chapter 2. The parameters tested in this research are substrates, thickness, and binder material. These were then compared with the battery performance to output a result showing the relationship of adhesion strength on battery performance.

1.4 Significance of Research

The thick electrode application has great potential to be the next-generation batteries for future electric vehicles. If this field is developed successfully, not only electric vehicles will be commercialized, but also the emissions caused by internal combustion engine-powered cars could be largely reduced and can produce a cleaner environment. The contemporary issue of high-cost production and low battery performance can indeed be addressed, and my conducted study will support future researches.

In creating electrodes, obtaining good wetting and adhesion of the electrode dispersion to the current collector foil is essential for achieving high capacity and good long-term performance. In producing these thick electrodes, improper adhesion may be caused due to various reasons including generation of internal stress, mismatch of surface energies, etc. In this paper, I have analyzed the relationship between multiple battery production parameters and the corresponding adhesion strength. The battery performance is also provided to show how adhesion strength varies with performance. This data will advocate future researches conducted on thick electrodes and will provide accurate data for each parameter.

1.5 Overview of Thesis

This thesis includes 4 chapters. Chapter 1 introduces the concept of LIBs, limitations of contemporary LIBs, a solution proposed, and the introduction to my research and contributions. Chapter 2 provides the experimental procedures performed in this research. A detailed outline is documented including each material synthesis, facilities used for material characterization, procedures for mechanical peel test, procedures for constructing each battery cells, as well as procedures for battery performance test. Chapter 3 discusses all the results outputted from Chapter 2. It introduces the comparison between the thin and thick electrodes, validating the limitations of current thick electrodes, followed by a detailed analysis of peel test and performance results. Chapter 4 concludes and summarizes the thesis, mentions contributions, and suggestions for future works for this research.

Chapter 2. Experiments

2.1: Preliminary Experiment

I conducted a preliminary experiment comparing a thin cathode commonly used in commercial batteries and a thick cathode. The active material used was LCO, a mixture of Li_2CO_3 and $CoCO_3$ was used in the production of both electrodes. The porosity maintained equally between the two electrodes as well. The only difference was the thickness. The thin cathode was 50 µm and the thick cathode was 190 µm. The methodology and the procedure used is the same as Section 2.2, but only with different materials as shown above. The electrochemical testing was completed to output (1) Rate Capability test results at 0.1C, 0.2C, 0.5C, 1C, 2C, 3C, and 5C, (2) Cycle life test results from 0-100 cycles.

Figure 9 compares two electrodes for discharge capacity at increasing cycle numbers. Discharge capacity measures the battery performance by calculating the discharge current by the capacity of the material and cycle number measures battery life. As seen in green, the thin electrode remains consistent throughout the increased cycle numbers and keeps a capacity retention rate of 78.55%. The thick electrode is shown in purple and shows a tremendous decrease as the cycle number increase. Figure 10 shows a similar result. This provides a rate capability comparison by plotting discharge capacity as C-rate increases. C-rate is a measure of how fast a cell is charged/discharged. This also shows a decreasing trend for the thick electrode, almost reaching zero for C-rates higher than 5C.

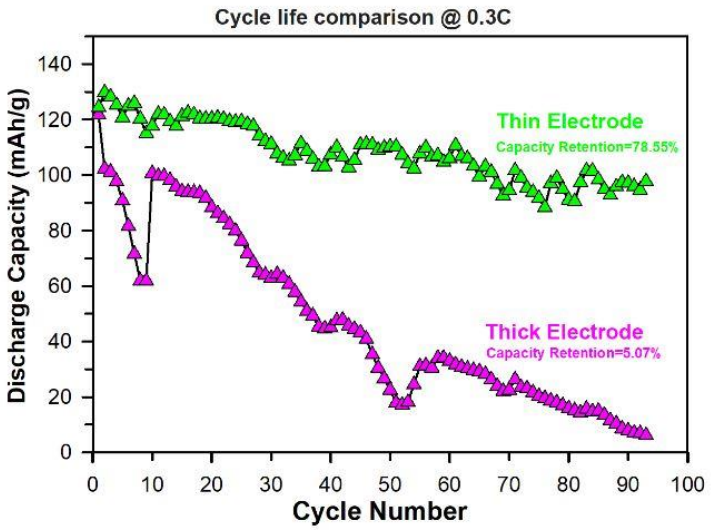

Figure 9. Preliminary Experiment: Cycle Test

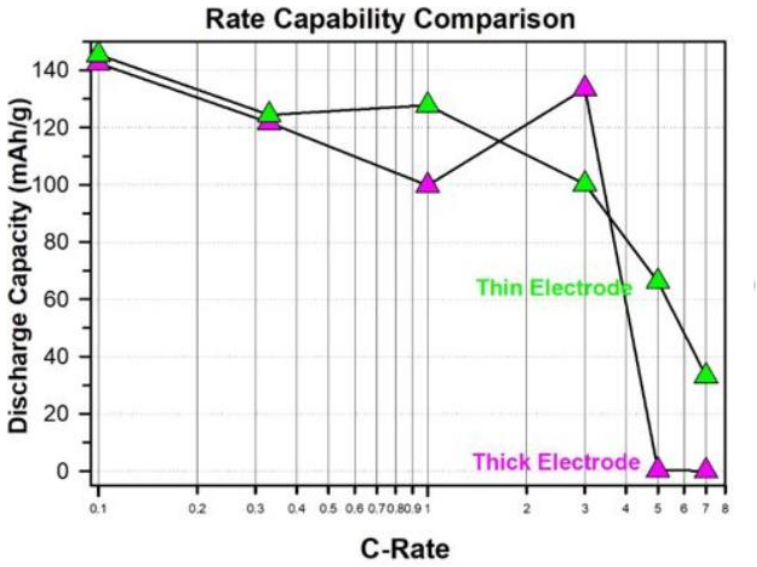

Figure 10. Preliminary Experiment: Rate Capability Test

The data outputted showed that contemporary thin electrodes perform better than thick electrodes. This data proved the limitations of conventional thick electrode applications, thus proving crack formation is required to enhance the performance for thick electrodes.

2.2: Methodology

To keep consistency, commercial LFP powder, $LiFePO_4$ (MTI Corp.) was used as the active material for all the experiments. The weight ratio of 85:7.5:7.5 was used for the active material, binder, and the carbon material correspondingly. The materials were added in stages to ensure proper dispersion of binders and carbon around the active material. For each experiment, 7.5 percent of each binder material and 1.0 mL of solvent. An additional amount of solvent was added appropriately to ensure good viscosity. A Zirconia ball was added then mixed using Thinky Mixer, shown in Figure 11, at a low RPM of 300-500 until the solution was almost fully clear.

Figure 11. Thinky ARV-310 Planetary Centrifugal Vacuum Mixer

Once this was finished, a 7.5 weight ratio of conductive carbon black consisting of super p, carbon nanofiber, and micro-graphite were added with the corresponding ratio of 5:1.5:1. Super P is nanometer-sized carbon used for electronic conductivity, micro-graphite is a micron-sized graphite for ensuring better carbon availability, and carbon nanofiber (CNF) is a cylindrical

nano-sized fibers for ensuring interparticle contact. The mix was then facilitated with the Thinky Mixer at a higher RPM of 700-1000. The mix was stopped and checked for the viscosity and if it was too viscous, 0.5 mL of solvent was added each time. Once the material was properly mixed at a reasonable viscosity by visibility, the remaining 85 percent of active material was added. The mixing process repeated, adding 0.5 mL of solvent material each time until the material was visibly viscous [7].

After the active material production, the substrate was prepared for use. For the substrate testing, a regular aluminum foil, carbon-coated aluminum foil, and surfaced etched aluminum foils were used. These were cut to an appropriate size and laid on a vacuum suction machine shown in Figure 12. The active material was poured onto the flat current collector and was adjusted for thickness using the doctor blade shown in Figure 13. The thickness was purposely adjusted as over twice the desired thickness in preparation for the next calendaring process. During the process of drying, the solvent evaporates which causes the thickness to shrink. Hence, we set the doctor blade thickness to a higher value.

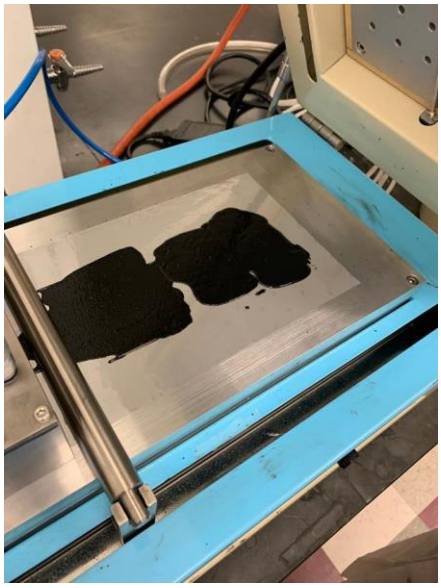

Figure 12. Slurry Coating Process

Figure 13. Doctor Blade (MTI Corp.)

Once the slurry coated on the current collector was properly adjusted for the desired thickness, the slurry cast active material on the substrate was dried at 353 K for 30 minutes in a conventional oven and then at 393 K for 12 hours in a vacuum oven(Across Intl.). After the drying process, the material was taken to the calendaring machine.

Figure 14. Heat Rolling Press with Variable Speed (MTI Corp.)

Calendaring of electrodes, or heat-applied roll pressing is done in the battery fabrication process and is carried out after the coating and drying stage of fabrication. In this process, the electrodes are compacted to improve the volumetric energy density and rate performance of the electrodes and also improve the interparticle contact [8]. The rollers are heated to a temperature of 100˚C. The temperature improves the fluidity of the binder which makes the electrode more malleable. Results have indicated that the pressing of the electrodes increases the capacity retention at high rate, reduces the contact resistance, and results in a significant improvement to the cycling performance. The heat rolling press includes an adjustable knob for thickness. This was varied in the thickness testing and was pressed to the desired thickness. This process was completed as an attempt to reduce the porosity of the active material to ~40%. Electrodes were then cut into circular disks of 13.7 mm in diameter using an electrode punch (Hohsen).

Porosity was calculated using Equation 1 using apparent density and true density. True density was calculated as 3.1 g/cc for the material used in this study. The apparent density was measured by taking the weight of the electrode coated on the substrate, subtracting the substrate weight, and diving this number by the volume of the electrode

$$\text{Porosity} = \left(1 - \frac{Apparent\ Density}{True\ Density}\right) * 100$$

Equation 1. Porosity Equation

The next process consisted of the coin cell fabrication. The coin-type cells of the stainless-steel 2032 configuration (MTI Corp.) were assembled in an argon-filled LC Tech glove box. The prepared active material was used as the cathode, the lithium metal was used as the anode, and a 1M $LiPF_6$ in ethylene carbonate (EC)/ethyl methyl carbonate (EMC) by 1:1 weight

ratio (Gotion) as the electrolyte with a polypropylene separator of 25 μm thickness (Celgard 2500). The cells were assembled and sealed in an electric crimper (MTI Corp.).

Figure 15. Argon-filled Glove Box (LC Technology)

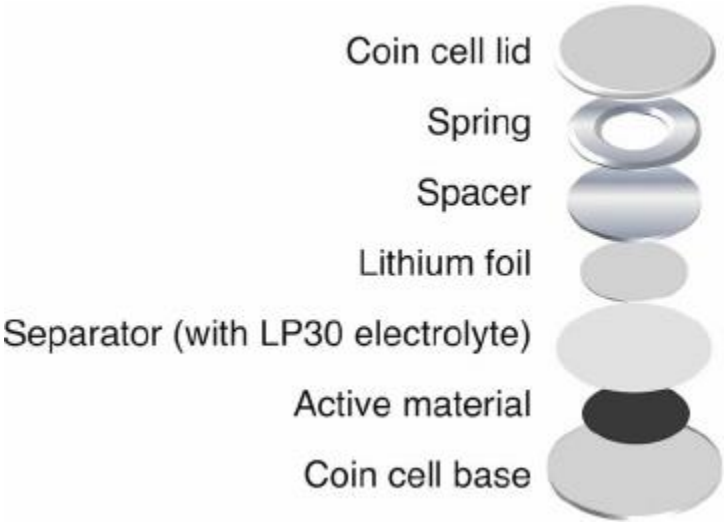

Figure 16. Coin Cell Production Schematic

The cells were rested for 1 day to allow electrolyte penetration into the bulk of the electrode. Then charge-discharge cycles performed in the potential range of 3-4.30 V in a multi-

channel battery tester (Arbin Instruments) at 298 K. The cells were initially subjected to two formation cycles to ensure the formation of SEI (Solid Electrolyte Interface) and good cyclability. For electrochemical performance, the rate capability test was performed.

Figure 17. Arbin Battery Cycler (Arbin Instruments)

The Arbin software was also used and each coin cell's C-rate, defined as the amount of time to fully charge/discharge a cell, and this was calculated using Equation 2 below.

$$1\text{C (Amps)} = \text{Active Mass (g)} * \text{specific capacity } \left(\frac{mAh}{g}\right) * \frac{1A}{1000mA}$$

Equation 2. Theoretical Capacity Equation

The testing was completed at these following C-rates: 0.1C, 0.2C, 0.5C, 1C, 2C, 3C, 5C to test for both low and high performance uses. The coin cells were initially subjected to two formation cycles to ensure the formation of SEI (Solid Electrolyte Interface) and good cyclability. The capacity and the specific capacity of each sample were also measured using Equation 3 and 4 to produce accurate data.

$$\text{Specific Capacity} = \frac{96.485\ C}{1\ mol} * \frac{1\ A * s}{C} * \frac{1000\ mA}{A} * \frac{1\ hr}{3600 s} * \frac{1 mole(ActiveMass)}{g}$$

Equation 3. Specific Capacity Equation

$$\text{Specific Capacity} = \frac{96.485\ C}{1\ mol} * \frac{1\ A * s}{C} * \frac{1000\ mA}{A} * \frac{1\ hr}{3600 s} * \frac{1 mole(LiFePO_4)}{157.5 g} = 170\ \text{mAh/g}$$

Equation 4. Specific Capacity Calculation for $LiFePO_4$

$$\text{Capacity} = \text{Specific Capacity} * \text{Active Mass}$$

Equation 5. Capacity Equation

2.3: Parameters

The parameters tested for this research are as followed: substrate, thickness, and binder material. The sample table provides the sample number for each parameter differed and will be used for a reference for the results.

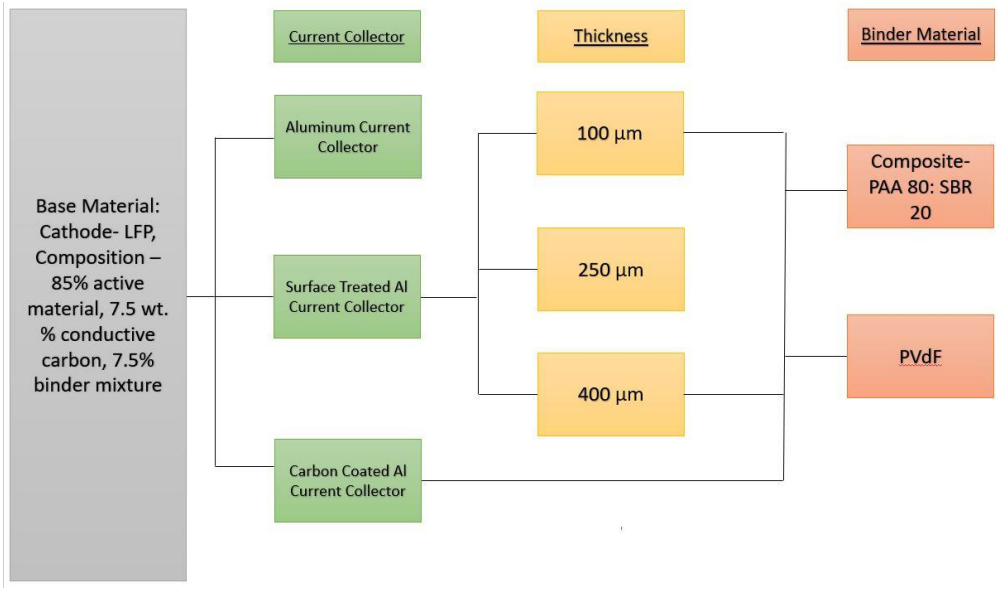

Figure 18. Design of Experiment

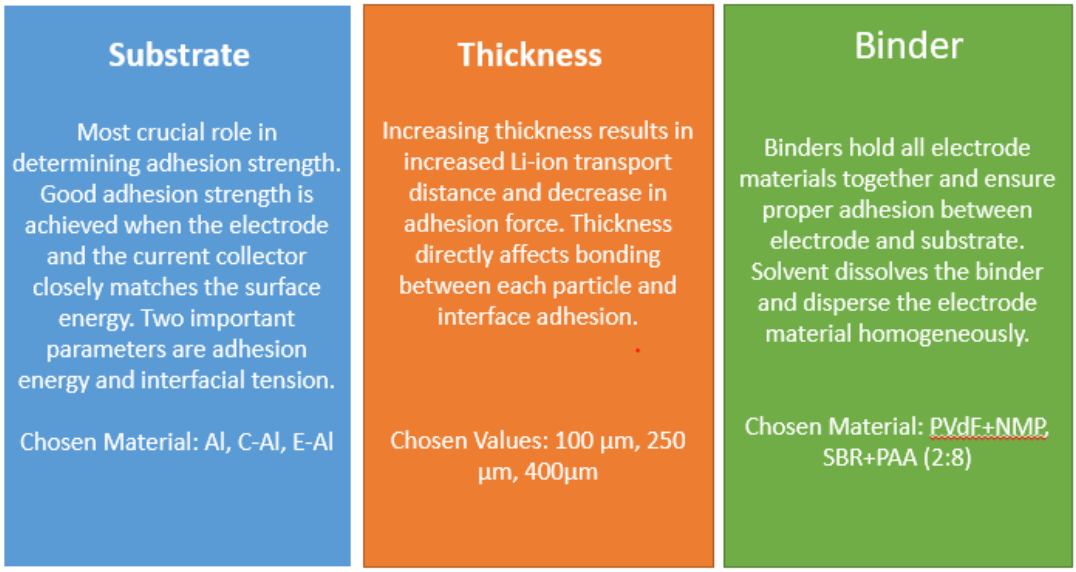

Figure 19. Effect of Each Parameter on Adhesion

Sample I was created for 100 µm on Al foil, but showed a complete mechanical delamination, disallowing further testing. Samples II and IV were used to compare the effect of substrate on adhesion force and performance. Samples III, IV, and V were used to compare the effect of thickness on adhesion force and performance. Samples VI, VII, VIII, and IX were used to confirm the thickness testing and to compare the effect of binders on adhesion force and performance.

Sample #	Binder	Substrate	Thickness (µm)
I	PVdF	Al	100
II	PVdF	C-Al	230
III	PVdF	E-Al	100

IV	PVdF	E-Al	220
V	PVdF	E-Al	340
VI	PVdF	C-Al	80
VII	PVdF	C-Al	340
VIII	SBR/PAA (2:8)	C-Al	80
IX	SBR/PAA (2:8)	C-Al	350

Table 1. Sample Table

2.3.1: Substrate

Substrate plays one of the most crucial roles in determining the adhesion strength of the electrode, especially at higher thicknesses. When the surface energy of the electrode slurry matches (is close to) the substrate-free energy, a good adhesion is achieved. In other words, the slurry should have a low contact angle (<90˚), and the substrate have a high wettability to ensure proper contact. Two important parameters in the characterization of adhesion between the coating and its substrate are adhesion energy and interfacial tension. Adhesion energy describes the initial adhesion between the coated layer and the substrate, while the interfacial tension determines the long-term adhesion.[4] The substrates used for this experiment include aluminum current collector (Al), carbon-coated current collector (C-Al), and surfaced etched/roughened current collector (E-Al). Bare aluminum foil is polished and has high surface energy. For thin electrode purposes and organic solvent-based slurries, it is suitable. It is also relatively low-cost. The C-Al foil has a layer of carbon on top of the Al substrate. This helps in ensuring good electronic conductivity and provides a degree of surface roughness. E-Al foil is made by etching

the surface of Al-foil using weak acids which remove some material and making the surface rougher.

The samples tested in this experiment are I, II, and IV. All parameters were kept constant except for the substrate. The thickness was held ~250 µm, the active material used was LFP, the binder material of PVdF and NMP, and with a weight ratio of 85 percent active material: 7.5 percent of binder material: 7.5 percent of conductive carbon black material. Each substrate was chosen with the purpose of observing adhesion strengths between current collectors.

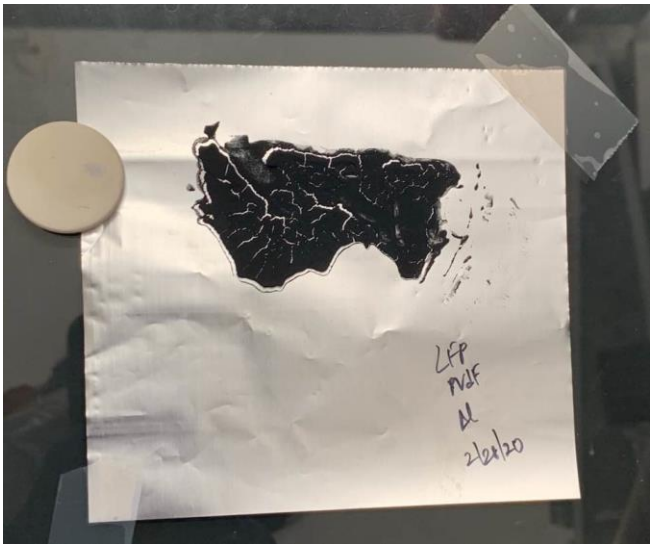

Figure 20. Sample I: Al Substrate

Sample 1 with aluminum current collector showed a complete delamination after the calendaring process was done. The active material used was proved to have insufficient adhesion strength and failed to stay attached to the regular Al substrate. This sample was disregarded in the results section and the data processing was curtailed.

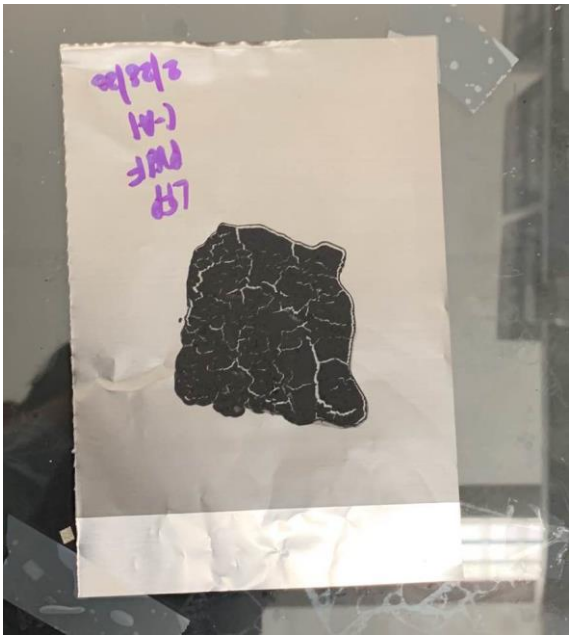

Figure 21. Sample II: C-Al

The C-Al sample displayed many visible cracks on the surface. The sample remained on the current collector and was tested for the adhesion force and electrochemical force as planned.

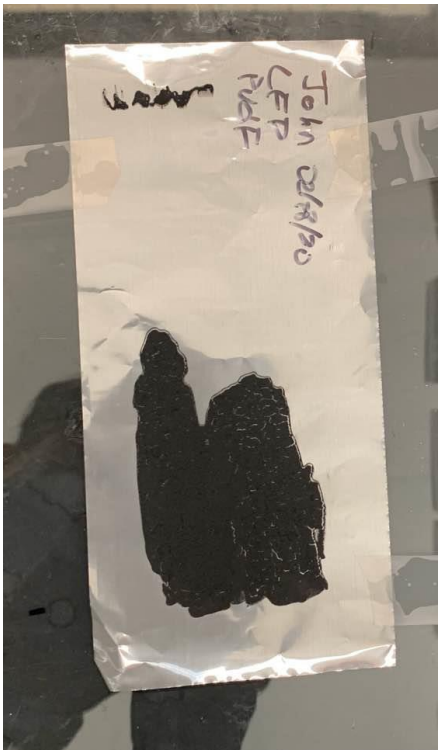

Figure 22. Example Sample: E-Al

Figure 21 shows an example sample of the E-Al. This sample was not used in this experiment due to the low thickness, rather sample IV was used to match the C-Al thickness and gather data for thick electrodes. This figure is provided to show the difference of how the coated material looks on the etched aluminum foil.

Thickness	Active Material	Binder	Weight Ratio
250 µm	LFP	PVdF +NMP	85:7.5:7.5

Table 2. Consistent Parameters for Substrate Testing

2.3.2: Thickness

The different thicknesses used in this experiment are ~100 µm, ~250 µm, ~400 µm. The constant parameters include LFP as the active material, PVdF, and NMP as the binder, 85:7.5:7.5 weight ratio, and E-Al as the substrate. The E-Al was used after gathering data of previous substrate testing, which displayed the E-Al accommodates the best adhesion force.

As briefly mentioned above, as the thickness increases, the Li-ion transport distance increases, thus worsening performance. The following thickness testing was chosen for the above values to observe the adhesion strength of these crack formed electrodes ranging from thin to thick electrodes. The thin electrodes are expected to perform better and contain better adhesion strength because of the strong bonding between each particle and better interface adhesion with the current collector. The thin electrode also has the ability to spread easier onto the current collector and increase adhesion strength, thus increasing interparticle contact and increasing electrode-substrate contact.

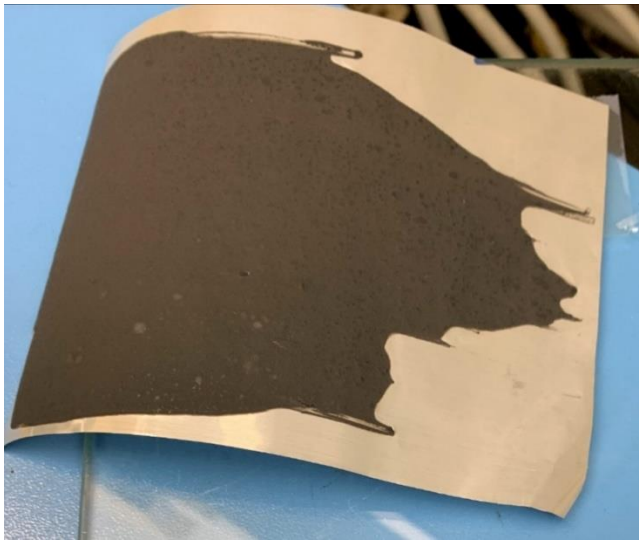

Figure 23. Sample III: 100 µm

Figure 24. Sample IV: 250 µm

Figure 25. Sample V: 400 µm

Substrate	Active Material	Binder	Weight Ratio
E-Al	LFP	PVdF +NMP	85:7.5:7.5

Table 3. Consistent Parameters for Thickness Testing

2.3.2: Parameters- Binder

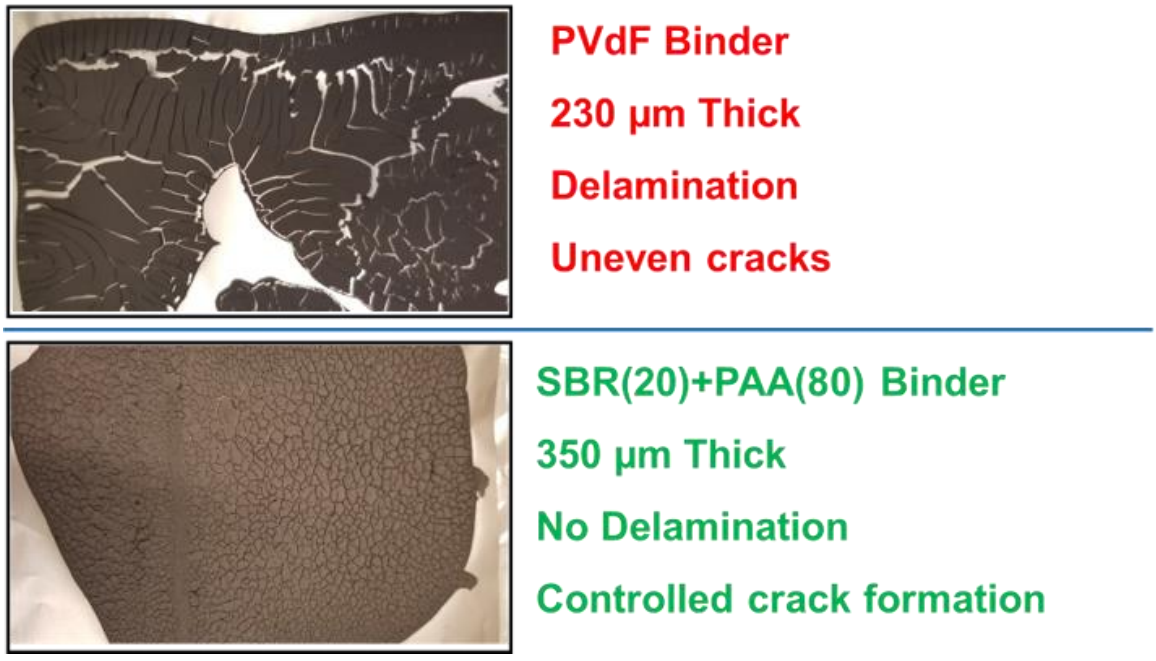

Figure 26. Binder Chemistry Samples

This data was received from the graduate student who contributed to this part of my research. The different binders tested were PVdF with NMP and the composite binder made of SBR (20): PAA (80). The samples were both made at 80 µm and 350 µm. For this set of experiments, the C-Al was used as a substrate. Binder materials SBR and PAA are aqueous solutions, and with water-based binders, the slurry (a form of active material in battery production) spreads easier on C-Al than E-Al.

In this section, we designed an experiment to see the effect of different binder-solvent systems on the mechanical properties of the electrode. Binders act as glue and hold all the electrode materials together and ensure proper adhesion between electrode and substrate. The solvent helps dissolve the binder and disperse all the electrode materials homogenously. Conventionally, PVdF binder has been used for its good electrochemical stability and offers fairly good mechanical properties. However, at increasing thicknesses, the PVdF binder is not able to offer the desired electrode stability. Furthermore, there is uncontrolled crack-formation and consequent delamination of the electrode. Hence, a different binder system was chosen. SBR and PAA mixed in specific ratios gave good mechanical properties and control over crack formation. These binders are water-soluble which makes the process environment friendly and affordable. Despite water-based slurries having higher surface energy, the SBR-PAA electrode shows better lamination.

Substrate	Active Material	Thickness	Weight Ratio
C-Al	LFP	350 µm 80 µm	85:7.5:7.5

Table 4. Consistent Parameters for Binder Testing

2.4: Mechanical Peel Test

The peel test is a conventional method in the battery industry for ranking the adhesion strength of electrodes, which separates the active material coating from the current collector using bond tapes [9]. In the peel test, the interface of delamination provides qualitative information about possible failure mechanisms in the electrodes [10]. The conventional mechanical peel test was performed using a micromechanical test system (MTS Tensile Strength Machine) to measure peeling forces. The peel test was done on a 0.5 in. wide and 2 in. long electrode sandwiched between two adhesion tape (3M VHB 4950 Heavy Duty Mounting Tape). Figure 27 shows the MTS Tensile Strength Machine experimented on a custom-designed setup. The adhesive tape was removed by peeling at an angle of 180° on the system with a load cell of 10 lbf at the rate of 0.025 in/sec. The force readings from the setup were obtained as voltage signals which were then converted to peel-force based on the load cell conversion factor.

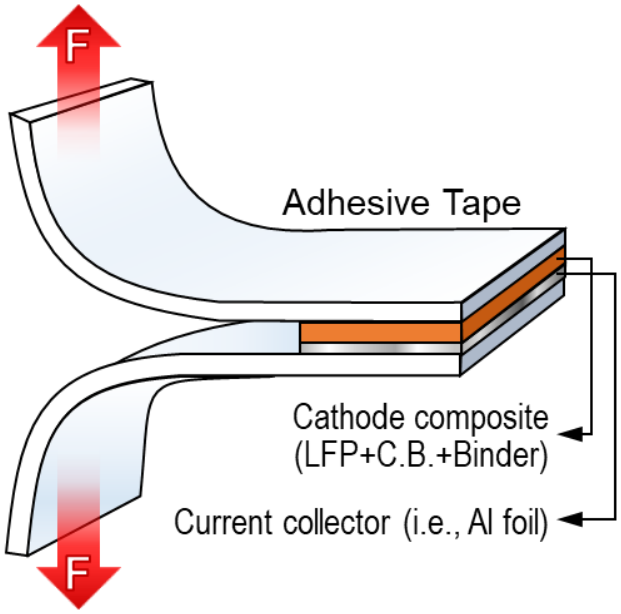

Figure 27. Peel Test Schematic

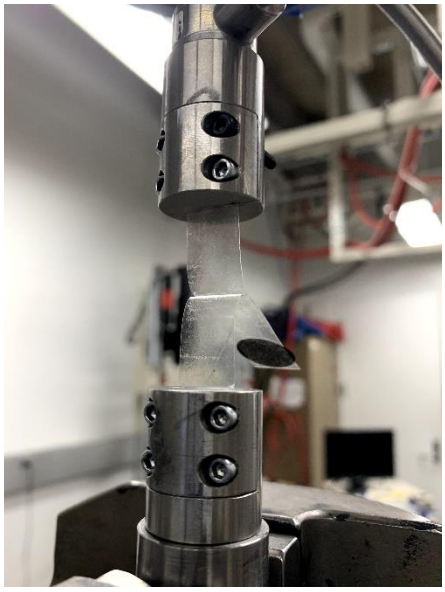

Figure 28. Tensile Strength machine and Test Set-Up

Chapter 3. Results and Discussions

3.1: SEM Test for Composite Binder

The surface morphological studies were carried out on a Hitachi model S-3000N SEM (Scanning Electron Microscope). This study was done on the composite binder consisting of SBR and PAA at 20:80 ratio.

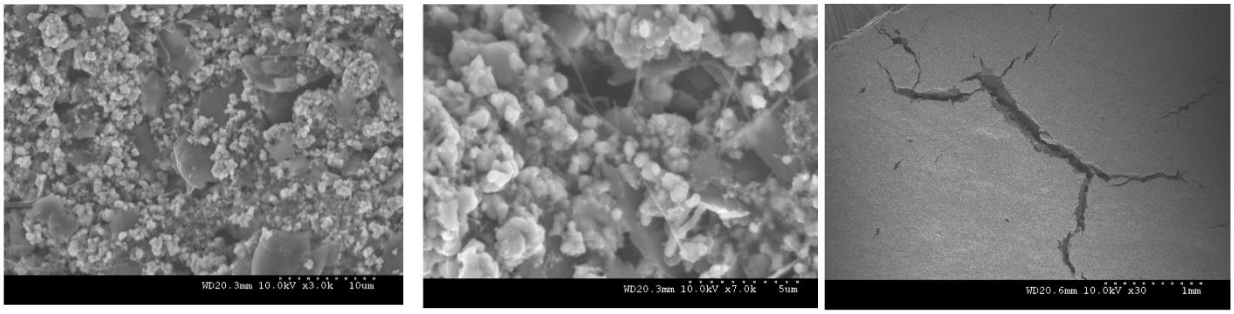

(a) (b) (c)

Figure 29. SEM image of LFP with Composite Binder scaled at (a) 10 μm (b) 5 μm (c) 10 mm

The SEM images give information about the porosity, material distribution, crack morphology, and the electrode surface. Figure 28 shows the composite binder images at different magnifications. The low magnification image shoes the LFP active material with the carbon binder distribution. The middle image shows the pores in between the electrode materials. These pores help in the electrolyte penetration into the bulk of the electrode. Large pores may cause cracks during the cycling of the electrode and loss of particle contact. Furthermore, carbon nanofibers can be seen as threads connecting particles. The third image shows the crack as seen from the top of the electrode. The crack width is approximately 50 microns after the calendaring process. The cracks seem to originate randomly when looked at from the surface, but there might be more information that could be obtained from other characterization studies to help explain the origin of these cracks.

3.2: Peel Test Results

The data below shows the results gathered from the mechanical peel test. The tensile strength machine used for this experiment outputted values in voltages which were normalized and converted to the peel-force based on the load cell conversion factor. The first part of the graph with high peaks is ignored because this data shows the tape being pulled off each other. The graph showing stable frequencies is when the active material is being peeled off the tape. These values are used and normalized as an average force and compared. Figure 29 shows an example of a converted graph acquired from the load cells.

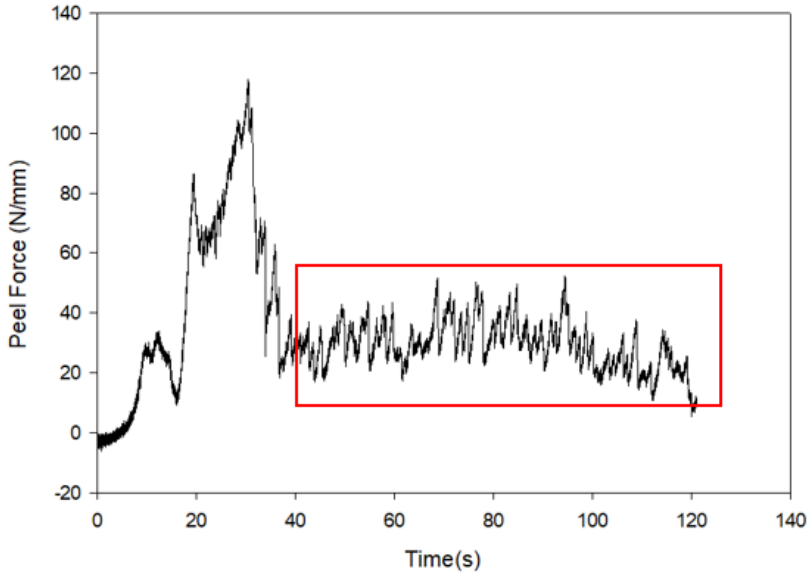

Figure 30. Sample Output from Peel Test

The test samples were tested and plotted on the graph below in figure 29. All of the data points were taken and normalized to peel-force measured in mN/mm, then compared with other samples. The type of substrate used is provided for each sample for better comparison. The first two bars on the graph show the data for samples II and IV, comparing the substrates, and the last

three bars show the data for samples III, IV, and V, comparing the thicknesses. Sample IV is provided twice for better visuals on each comparison. Unfortunately, the peel test was not performed on the binder testing due to the COVID-19 outbreak.

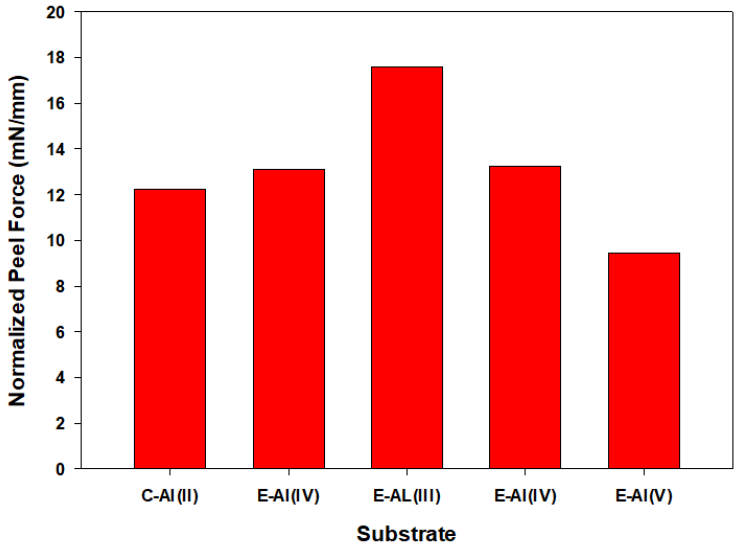

Figure 31. Peel Test Results

Samples II and IV show the difference of adhesion force of the same active material on different substrates. As mentioned above, the active material on the aluminum current collector completely delaminated, therefore this data was deemed idle. As expected, sample IV with the surfaced etched aluminum current collector showed to have the best adhesion force and match the surface energy with the LFP active material used. The material coated on the carbon-coated aluminum current collector also had similar adhesion strength and provided good data for comparison.

For samples III, IV, and V, the material with the lowest thickness is proved to have the most adhesion strength. This is due to the lower lithium-ion transport distance, therefore requiring less cracks, and the risk of having mechanical delamination. The samples outputted a stable data,

showing a steady decrease in adhesion force as the thickness increase. The thickness for each material was varied by 150 µm and the adhesion force was varied by nearly 4~5 mN/mm.

3.3 Electrochemical Results

The electrochemical performance was measured with the Arbin Cycler and the Arbin program and produced these following outputs. The voltage profile was plotted in variation of the capacity at low and high C-rates. The discharge capacity was also plotted with respect to each C-rates. The thickness and areal material loading of each cell are provided on the rate capability graph.

3.3.1 Substrate Testing

For this experiment, the thickness was kept the same as well as the areal loading, only differing the substrate material to provide accurate data to only compare the varied material. Figure 30 shows the discharge capacity values at different C-rates. This testing was completed at low and high C-rates to observe the degradation as the performance increases, and also to see variations. As seen in this figure, overall, the E-Al showed to have better discharge capacity up to 2C. However, the C-Al shows better performance for higher C rates from 3C to 5C. There may be many reasons why the C-Al showed better performance for high C-rates, one estimate being the additive conductive carbon material improved the electronic conductivity, resulting in this output for high C-rates. The discharge capacity at 1C rate for the C-Al was ~90 mAh/g and E-Al was ~100 mAh/g, having an 11.1% decrease, and showing only a slight difference in the performance. Also, the discharge capacity at 3C for C-Al was ~68 mAh/g and E-Al was ~69 mAh/g, having only a 1.47% decrease, and showing only a minuscule difference.

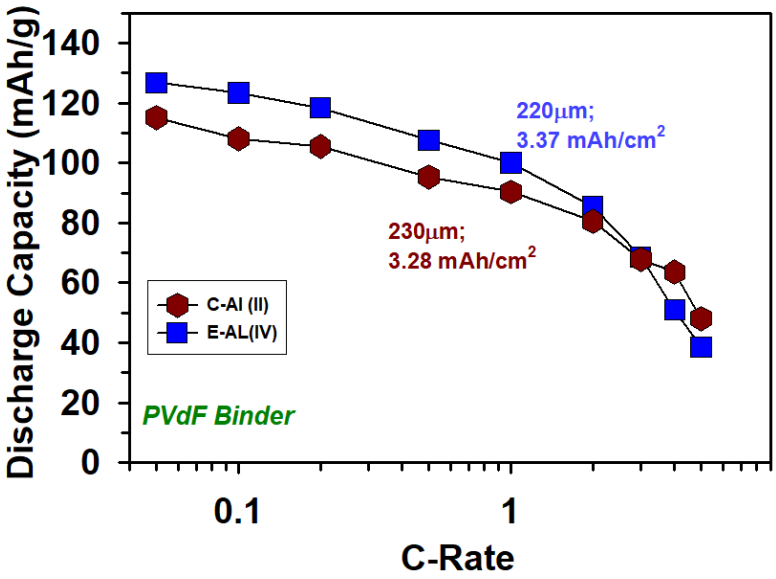

Figure 32. Substrate: Discharge Capacity vs. C-Rate Graph

The voltage vs. capacity graph shows the potential difference between the cathode and the lithium metal anode in the cell's charge and discharge cycles. Both samples showed to reach similar voltage potentials but showed a clear distinction in the capacity. These graphs provided for samples II and IV demonstrate that E-Al reaches higher capacity for lower C-rates, and C-Al reaches higher capacity for higher C-rates.

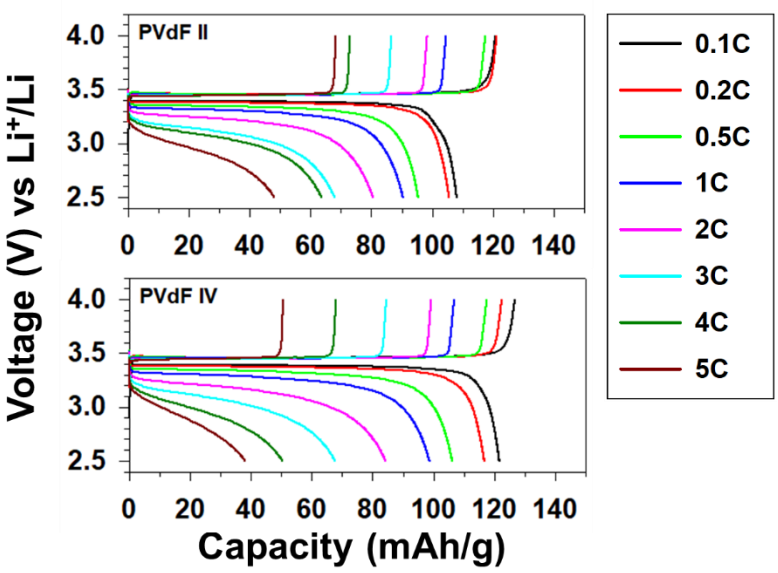

Figure 33. Substrate: Voltage vs. Specific Capacity Graph

The E-Al substrate proved to have slightly better adhesion force than the C-Al, but not showing too much of a difference, only differing ~1 mN/mm. The electrochemical testing provided promising data, showing a direct relationship between adhesion force and electrochemical performance. The E-Al showed to have better adhesion force and corresponded with better electrochemical performance. The slight force measurement difference corresponded with slight performance differences, and even showed that C-Al had better performance for higher C-rates. To provide a more in-depth analysis of the relationship of adhesion strength and battery performance, the following sections analyze the data for thickness and binder testing.

3.3.2 Thickness Testing

For this experiment, the E-Al substrate was used in accordance with the data outputted from the substrate testing, proving E-Al has better adhesion force. The thickness varied from thin to thick electrodes and each thickness and areal loading is provided in the C-rate graph. As expected, sample III, the thinnest material showed to have the best performance for low and high

C-rates, followed by sample IV, the next thinnest, and sample V, the thickest. The discharge capacity at 1C rate for 100 μm sample was ~123 mAh/g, the 250 μm sample was ~100 mAh/g, and the 400 μm was ~7 mAh/g, showing a dramatic decrease in performance as the thickness increased. From sample III to sample IV, it showed a decrease of 18.7%, and from sample IV to sample V, 93% decrease. The discharge capacity at 5C for the 400 μm even reached 0 mAh/g. This data proves that simply increasing the thickness has limitations.

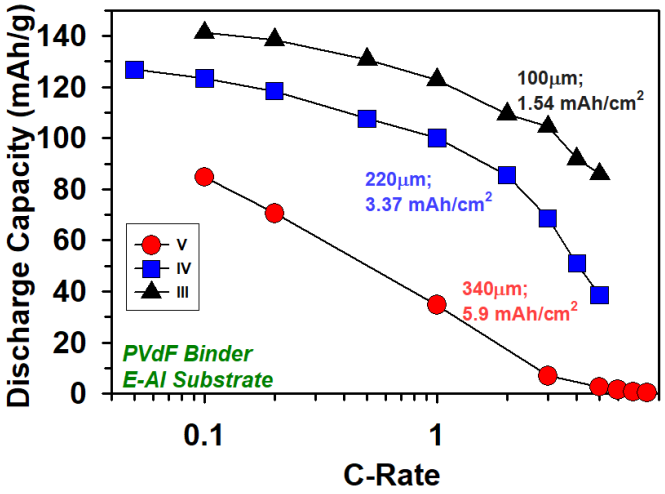

Figure 34. Thickness: Discharge Capacity vs. C-Rate Graph

Figure 34 provides the voltage potential for each sample. These graphs give a clear visualization and distinction between the samples. Samples III and IV showed to reach similar voltage potentials for both low and high C-rates, but sample V showed to produce no voltage potential for high C-rates. The capacity limit also is visibly clear. Sample III reaches high capacity for low and high C-rates, sample IV shows less, and sample V shows very low or no capacity.

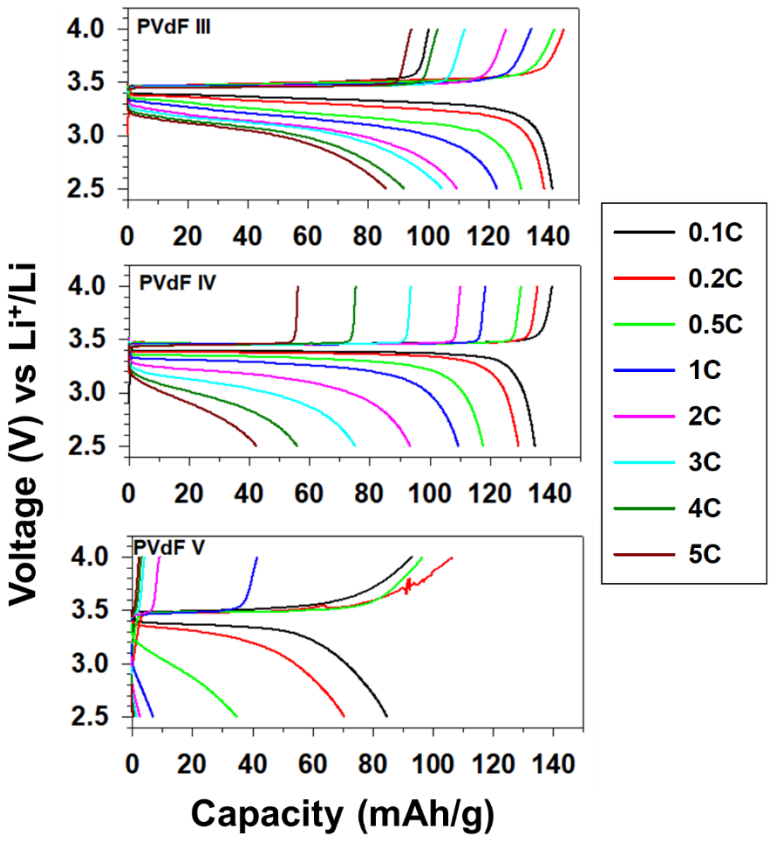

Figure 35. Thickness: Voltage vs. Specific Capacity Graph

The electrochemical performance showed very promising data with respect to the adhesion force data. The peel test data for thickness testing showed that as the thickness increased, the adhesion force decreased. The same trend is shown here for the performance test, confirming as thickness increased, the performance worsened. This data, combined with the substrate result, shows that adhesion force has a correlation with electrochemical performance.

3.3.3 Binder Testing

For this experiment, the C-Al substrate was used because the binder materials SBR and PAA are water-soluble and the slurry material pours easier on C-Al than E-Al. It was deemed sufficient to

use the C-Al after observing the adhesion force and performance results, showing only a slight difference between the two. Unfortunately, for the binder testing, the mechanical peel test experiment could not be completed due to the COVID-19 outbreak. Only the performance results are provided, but still shows a promising data. For this binder testing, the thin and the thick electrode materials of different binder materials were tested. As shown in Figure 35, the thin electrode at 80 μm shows better performance than the thick electrode 350 μm, validating the results for the thickness testing.

For performance, the material consisting of PVdF and NMP binder showed to have better performance for the thin electrode, but the relationship differed for thick electrodes. The discharge capacity at 1C rate for the thin electrode consisting of PVdF was ~128 mAh/g and the composite binder was ~109 mAh/g. The discharge capacity at 1C rate for the thick electrode consisting of PVdF was ~33 mAh/g and the composite binder was ~39 mAh/g. Again, the discharge capacity at a 5C rate for both binder materials reached 0 mAh/g.

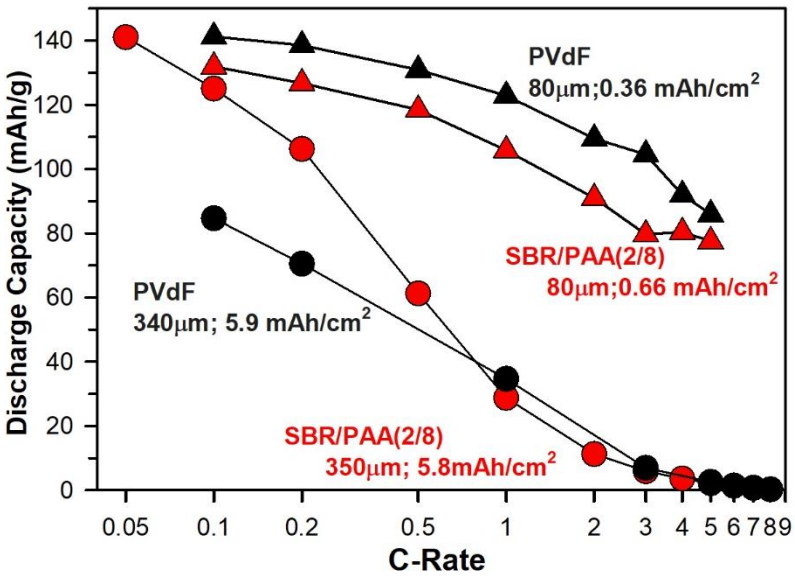

Figure 36. Binder: Discharge Capacity vs. C-Rate Graph

Figure 36 provides the voltage potentials for each sample. The thickness variation has the same results as the thickness testing. The voltage potential was much lower, and the capacity limit was lower for thicker electrodes. For thin electrodes, the voltage potential followed the same trend as the C-Rate graph. The PVdF showed to have higher capacity limits than the composite binder for low and high C-rates.

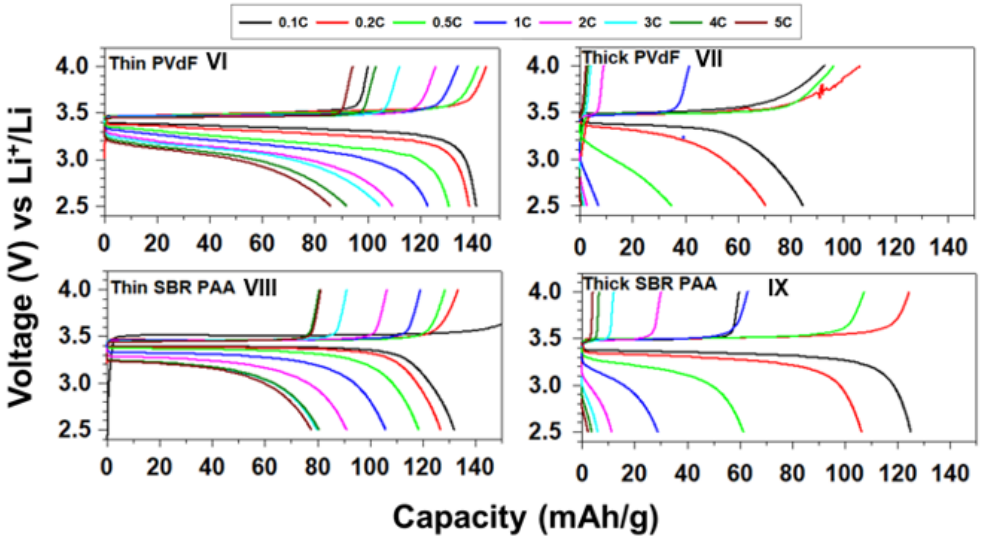

Figure 37. Binder: Voltage vs. Specific Capacity Graph

Initially, this binder testing was planned for the use of comparing adhesion force on electrochemical performance for varying binders. However, the peel test was not able to be completed. The results from this testing does confirm that as thickness increases, the performance decreases.

Chapter 4. Conclusion

4.1 Summary

In thick electrode applications, it is important to create physical channels to allow the electrolyte to penetrate the bulk of the electrode and enhance performance. This research implied the in-situ crack formation in the use of thick electrodes and analyzed a big issue of these crack generation, the potential mechanical delamination of the electrode from the substrate. This mechanical delamination can result in capacity loss and a shortage of cells. The different types of parameters used for generating these cracks were tested to observe the electrode-substrate adhesion force with battery performance. For the substrate testing, the E-Al showed to have slightly better adhesion force, and showed a direct relationship in performance, having slightly better performance than the C-Al. For thickness testing, the peel test data showed as thickness increased, the adhesion force decreased. The same trend was provided for the performance test. For binder testing, the peel test could not be done, but a decrease in performance as an increase in thickness was confirmed.

With only one sample tested for each testing, it's difficult to make a conclusion of this research based on the results for one sample. Therefore, for future research, more samples of the same materials will be tested for statistical variation. Also, to test the exact adhesion force between the electrode and the current collector, the tensile strength machine used for the mechanical peel test has to completely peel off the cathode composite material off of the substrate. If this is not the case and the cathode material remains on the current collector, this provides inaccurate data for the adhesion force and could provide results for cohesive forces of cathode material instead.

Therefore, for future research, the mechanical peel test will be performed multiple times to decide whether this is testing for the cohesive force of the active material or the adhesive force between the active material and the current collector.

This study includes limitations as described above and can't give an exact answer on whether the effect of adhesion force is related to the performance results. However, by addressing those limitations of this study and putting more time into more experiments and acquiring those results, the relationship of adhesion force or even cohesive force (if the peel test is confirmed to test cohesive forces, not adhesive) and the performance of each material.

4.2 Contribution

The issues of current commercialized LIBs are the under-utilization of active material and the high cost of production. The thick electrode with crack formation applications will continue to be studied and researched. My analysis of the effect of adhesion strength on battery performance will advocate future researches on thick electrodes and provide a complete database for each binder material, thickness, substrate, etc. This will further advocate researches being completed on thick electrodes, as well as a crack formed thick electrode by providing limitations of each parameter and the most optimal parameters to be used for testing. This study will provide a stepping stone for future researches conducted on using a mechanical peel test to acquire adhesive/cohesive forces once this research is complete.

4.3 Future Work

The future work immediately required for this research involved the mechanical peel test of the binder testing. This will further prove the effect of adhesion strength on battery performance. An experiment on water-soluble binders coated on E-Al and C-Al should be performed to prove that material made of soluble binders pours easier on C-Al and that C-Al has shown better adhesion strength. More experiments could be done on various parameters such as viscosity and perform the same testing. The same electrodes will be produced again, and the same mechanical peel test and electrochemical performance will be measured to observe the statistical variation. The atomic force microscopy test will be performed to measure Young's modulus of each material. More SEM images will be observed at cross-sectional areas to see adhesion between electrode and current collector. More substrates will be designed to improve adhesion by acquiring better surface properties. The scaling of electrode fabrication using the roll to roll test will be performed to determine adhesion strength. These additional experiments will strengthen the information that adhesion strength indeed has a direct relationship with battery performance.

Bibliography

(1) Park, J.-K. *Principles and Applications of Lithium Secondary Batteries*; Wiley-VCH Verlag & Co., 2012.

(2) Du, Z.; Wood, D. L.; Daniel, C.; Kalnaus, S.; Li, J. Understanding Limiting Factors in Thick Electrode Performance as Applied to High Energy Density Li-Ion Batteries. *J. Appl. Electrochem.* **2017**, *47* (3), 405–415. https://doi.org/10.1007/s10800-017-1047-4.

(3) Thorat, I. V.; Joshi, T.; Zaghib, K.; Harb, J. N.; Wheeler, D. R. Understanding Rate-Limiting Mechanisms in LiFePO4 Cathodes for Li-Ion Batteries. *J. Electrochem. Soc.* **2011**, *158* (11), A1185. https://doi.org/10.1149/2.001111jes.

(4) Kuang, Y.; Chen, C.; Kirsch, D.; Hu, L. Thick Electrode Batteries: Principles, Opportunities, and Challenges. *Adv. Energy Mater.* **2019**, *9* (33), 1901457. https://doi.org/10.1002/aenm.201901457.

(5) Lee, B.-S.; Wu, Z.; Petrova, V.; Xing, X.; Lim, H.-D.; Liu, H.; Liu, P. Analysis of Rate-Limiting Factors in Thick Electrodes for Electric Vehicle Applications. *J. Electrochem. Soc.* **2018**, *165* (3), A525–A533. https://doi.org/10.1149/2.0571803jes.

(6) Son, B.; Ryou, M.-H.; Choi, J.; Lee, T.; Yu, H. K.; Kim, J. H.; Lee, Y. M. Measurement and Analysis of Adhesion Property of Lithium-Ion Battery Electrodes with SAICAS. *ACS Appl. Mater. Interfaces* **2014**, *6* (1), 526–531. https://doi.org/10.1021/am404580f.

(7) Bitsch, B.; Dittmann, J.; Schmitt, M.; Scharfer, P.; Schabel, W.; Willenbacher, N. A Novel Slurry Concept for the Fabrication of Lithium-Ion Battery Electrodes with Beneficial Properties. *J. Power Sources* **2014**, *265*, 81–90. https://doi.org/10.1016/j.jpowsour.2014.04.115.

(8) Oladimeji, C. F.; Moss, P. I.; Weatherspoon, M. H. Analyses of the Calendaring Process for Performance Optimization of Li-Ion Battery Cathode. *Hindawi* **2016**, *2016*.

(9) Luo, H.; Zhu, J.; Sahraei, E.; Xia, Y. Adhesion Strength of the Cathode in Lithium-Ion Batteries under Combined Tension/Shear Loadings. *R. Soc. Chem.* **2018**, *8* (3996).

(10) Gaikwad, A. M.; Arias, A. C. Understanding the Effects of Electrode Formulation on the Mechanical Strength of Composite Electrodes for Flexible Batteries. *ACS Appl. Mater. Interfaces* **2017**, *9* (7), 6390–6400. https://doi.org/10.1021/acsami.6b14719.